Abstract

Title of Document: Heat Transfer and Pressure Drop Characteristics of a Manifold Microgroove Aerospace Condenser

David Boyea, Masters of Science 2013

Directed By: Michael Ohadi, Professor

Department of Mechanical Engineering

High performance condensers are an essential component in many energy conversion, electronics and process systems. Increased capacity and functionality with less and less available space has been a main driving force for development of smart condensers in energy systems. A literature survey of microchannel condensation shows that microchannels are useful for enhancing condensation heat transfer. Our previous work in this area has demonstrated that manifold microgroove heat exchangers operating in single-phase or two-phase modes offer substantially higher heat transfer performance with a greatly reduced pumping power when compared to state-of-art microchannel heat exchangers. Out previous microchannel condensation experiments ~~was using~~ have involved use of small scale manifold microgroove condensers (7 cm^2 base area) and a manifold microgroove condenser of this size and capacity has not been investigated before. The goal is to enhance heat transfer performance while minimizing the pumping

power, volume and weight. A compact lightweight manifold microgroove condenser, with 60 x 600 micron microgrooves and cooling capacity of 4kW, was fabricated, assembled and tested using two different manifold designs. Experiments using R134a and R236fa as working fluids and two different refrigerant side manifolds were performed. Overall heat transfer coefficient and the pressure drop across a manifold microgroove condenser were calculated and refrigerant side heat transfer coefficient was determined based on water side heat transfer coefficient. 4kW capacity was achieved with an LMTD of 8C. The manifold geometry was found to have a large effect on pressure drop and heat transfer performance as well as flow distribution. A majority of the pressure drop was found to be in the manifold creating poor flow distribution. Future work should focus on optimization of the refrigerant manifold design to reduce pressure drop, increase heat transfer and flow distribution as well as explore the effect of microchannel geometry. Unfortunately current stage of development CFD optimization techniques does not allow optimization of two-phase flow system. An optimization of the airside surface and manifold geometry of heat exchanger that potentially will be coupled with high performance condenser has been performed. It has been concluded that for high performances of single phase flow manifold flow area has to be comparable to microgrooves flow area.

HEAT TRANSFER AND PRESSURE DROP CHARACTERISTICS OF MANIFOLD MICROGROOVE AEROSPACE CONDENSER

By

David Boyea

Thesis submitted to the Faculty of the Graduate School of the
University of Maryland, College Park, in partial fulfillment
of the requirements for the degree of
Masters of Science
2013

Thesis Committee:

Professor Michael Ohadi, Chair

Professor Marino di Marzo

Professor Jungho Kim

Dedication

To my parents John and Debbie Boyea, I would not be who I am without your support and love.

Acknowledgements

First I would like to thank Dr. Michael Ohadi for his guidance through my graduate studies both in and out of the lab.

I would like to thank Dr. Serguei Dessiatoun for his mentoring in experimental techniques, fabrication and trouble shooting.

I would like to thank Dr. Amir Shooshtari for his help with technical writing and presenting my data.

Lastly I would like to thank all of the students I have worked with at SSTS, Raphael Mandel, Meera Mahadevan, Josh Fody, Harish Ganapathy, Rohit Andhare and Vibhash Jha. They all contributed in some way to helping me get to where I am and it was a pleasure working with all of you.

Table of Contents

List of Figures

List of Tables

Nomenclature

T_{win}	Inlet Water Temperature [C]
T_{wout}	Outlet Water Temperature [C]
T_{rin}	Inlet Refrigerant Temperature [C]
T_{rout}	Outlet Refrigerant Temperature [C]
T_{sat}	Refrigerant Saturation Temperature [C]
Q_{cond}	Condenser Cooling Capacity [W]
A	Condenser Area [m^2]
h_{ref}	Refrigerant Side Heat Transfer Coefficient [W/m^2K]
h_w	Water Side Heat Transfer Coefficient [W/m^2K]
C_{pwater}	Specific Heat of Water [J/kgK]
m_{ref}	Refrigerant Mass Flow Rate [kg/s]
m_w	Water Mass Flow Rate [kg/s]
LMTD	Log Mean Temperature Difference [C]
L	Length of Heat Exchanger Tube [m]
k_{al}	Thermal Conductivity of HX Tube [W/mK]
X	Vapor quality [-]
h_{fg}	Refrigerant Latent Heat of Vaporization [kJ/kg]
U	Overall Heat Transfer Coefficient [W/m^2K]
Cp	Specific Heat of Refrigerant [kJ/kg-K]
K	Thermal Conductivity [W/m-K]
Re	Reynolds Number [-]
H_{ch}	Microchannel Height [μm]
Alph	Aspect Ratio [-]
W_{chn}	Microhannel Width [μm]
W_{in}	Manifold Inlet Width [μm]
H_{man}	Manifold Height [μm]
N	Number of Passes
W_{man}	Manifold Width [μm]
P_{sat}	Saturation Pressure [kPa]
μ	Viscosity [kg/m-s]
σ	Surface Tension [N/m]
P	Density [kg/m^3]

CHAPTER 1: Introduction

1.1 Motivation of the study

Most recent research has focused on the increase in performance of heat sinks and evaporators. However condensers are a very important part of thermal management systems and should also be considered when looking to improve the performance of a thermal management system. Condensers are critical components in two-phase thermal management systems for diverse energy conversion applications. 60% to 80% of an aircraft thermal load is comprised of electronic cooling (Swain, E.F, 1998). As electronics become increasingly more functional (higher electronics density) and more compact high efficiency thermal management systems will be required to deal with increased capacity and decreased allowable footprint. Single phase forced convection is a desirable method as long as the surface heat flux does not exceed 600w/cm^2 (Mahefkey, T., Yerkes, K., Donovan, B., and Ramalingam, M, 2004). The advantages of these types of systems are that they are simple, easy to construct and cost effective. However, single phase performance is limited by the material thermal conductivity and specific heat that they are constructed with. It is anticipated that the cooling demand of direct energy weapons and solid state lasers will exceed the capabilities of single phase forced convection thermal management systems. Two phase systems are more compact and have lower thermal resistance than the single phase systems. Multi-phase systems offer the best performance to deal with high heat fluxes in future electronic systems. In addition to aerospace thermal systems high performance condensers have applications on

industrial platforms. In 2011 the industrial sector accounted for one third of the United States energy consumption (U.S. Energy Information Administration, 2012). Energy efficiency in this sector is going to be an important part of research in the future with decreasing supply and increasing cost of natural gas and other fossil fuels. In addition thermal loads of electronics and power devices are becoming larger and larger forcing the capacity of thermal management systems to increase.

There have been many studies looking in to the heat transfer and pressure drop characteristics of two phase condensing flow in micro channels. Microchannels offer increased performance without adding significant weight or volume when compared to plate and fin or tubular heat exchangers. As the hydraulic diameter of the channels reduces the heat transfer enhancement increases but so do the pressure drop along the channel and the pumping power. Use of a manifold can reduce the pumping power drastically while allowing for increased heat transfer performance. The manifold reduces the pumping power by making one long microchannel in to many shorter microchannels in parallel which reduces the pumping power by 1/n where n is the number of microchannels. In addition, the short flow length ensures that the flow is always in the developing region which creates turbulent flow and better heat transfer.

1.2 Research Goals

The main objectives of this research project are as follows

- Determine pressure drop and heat transfer characteristics of a force fed manifold microgroove condenser for two different refrigerant manifolds using two different working fluids (R134a and R236fa)

- Determine performance of the condenser for different operating conditions, pressure, refrigerant flow rate and inlet quality.
- Optimize air side surface and manifold geometry using CFD code and metamodel optimization.

1.3 Organization of Thesis

Chapter 2 will provide a literature survey on reported results of other microchannel condensation heat transfer studies. Chapter 3 will discuss the experimental setup, force-fed design, test section, experimental, procedure and design of test parameters. Chapter 4 will discuss the results from the experiments, explain trends in the data and offer insight into the behavior of the condenser. Chapter 5 will go over the airside optimization that was performed and discuss the results. Chapter 6 will provide summary and conclusions, as well as discuss the suggested future work in order to expand the current study and enhance understanding of the related condensation phenomena.

Chapter 2: Literature survey

Condensing flow in mini channels and microchannels has been the focus of numerous experimental studies. A literature survey of experimental studies performed for minichannel and microchannel heat transfer condensation is presented in this chapter in order to gain further understanding and provide a comparison for our results.

2.1 Single Channel Studies

Cavallini et al conducted experiments using HFC R134a, R125 R32 R410A and R236ea measuring pressure drop and heat transfer coefficients over a range of mass flux's, mean vapor qualities and saturation temperatures of 100 to 750 kg/m^{2}s, 0.15 to 0.85 and 30°C to 50°C respectively in a single 8mm diameter smooth tube. For a given fluid and saturation temperature, 40°C, heat transfer coefficient and pressure drop increased with increasing mass flux and mean vapor quality. For a given mass flux the increase in heat transfer and pressure drop are linear with respect to vapor quality. However when vapor quality is kept constant and mass flux is changed the pressure drop penalty is different for high and low pressure fluids. (Cavallini, A. Censi, G. Del Col, D. Doretti, L. Longo, G.A. Rossetto. L, 2001)

Liu N, et al conducted experiments of heat transfer and pressure drop in single square and circular microchannels with hydraulic diameters 0.952 and 1.152 mm, heat transfer lengths of 0.352 and 0.336 respectively. R152a was used as the working fluid for all of the tests. The effect of saturation temperature, mass flux and quality are explored by varying these parameters between 40-50C, 200-800 kg/m^{2}s and 0.1-0.9 respectively as well as the effect of channel geometry. For a given quality and channel geometry heat transfer and pressure drop increased with increasing mass flux. For all channels and mas

fluxes heat transfer and pressure drop increased with increasing average quality. For low mass fluxes the square channel has better heat transfer than the circular channel because surface tension forces are dominant over shear forces which draws the liquid to the corners and lowers the thermal resistance. As mass flux increases shear forces take over and surface tension plays less of a role, as a result the enhancement effect of the square channels is reduced at higher mass fluxes. (Na Liu, Jun Ming Li, Jie Sun, Hua Sheng Wang, 2013)

Al-Hajri E., Shooshtari AH, Dessiatoun S and Ohadi MM conducted heat transfer and pressure drop experiments on a high aspect ratio single copper microchannel having dimensions of 2.8mm height, 0.4mm width (aspect ratio =7:1) giving a hydraulic diameter of 0.7mm. R134a and R245fa were used as the working fluids, the effects of saturation pressure; mass flux and degree of super heat, over the ranges of 30-70C, 50-500kg/m^2s, 0-10C, on pressure drop and heat transfer performance were investigated. For a given saturation pressure and 0 degree superheat the heat transfer and pressure drop increased with mass flux. These trends were due to increasing length of the annular flow region and increased convection from higher liquid and vapor velocities. The increase in pressure drop is mostly due to the lower vapor density which increases the vapor velocity. Surface tension is also affected by surface tension and liquid viscosity however they play a lesser role compared to the vapor density. Heat transfer and pressure drop decrease with increase in saturation temperature due to the increase in vapor density with the increase in system pressure. As the system pressure is raised the specific volume decreases which means the density increases. Degree of super heat had very little effect

on heat transfer or pressure drop compared to saturation temperature and mass flux. (E Al-Hajri, at all, 2013)

2.2 Multichannel Heat Exchanger Studies

Park, YC and Hrnjak P conducted heat transfer and pressure drop experiments using CO2 as the working fluid and characterized the heat transfer and pressure drop performance over different mass fluxes, saturation temperatures, inlet qualities and heat fluxes. The test section was made of extruded aluminum and had 10 channels each with a hydraulic diameter of 0.89mm. Heat transfer coefficient and pressure drop increased with increasing mass flux and vapor quality, however it should be noted that the pressure drop experiments were conducted with no heat transfer. Heat transfer is slightly higher at lower saturation temperatures however the effect is not as prominent as in previous studies. (Chang Yong Park, Pega Hrnjak, 2009)

Kim, Kim and Mudawar conducted a two part study characterizing the heat transfer and pressure drop performance of FC-72 refrigerant vapor condensing in 1.0 x 1.0mm channels. Tests were run over different refrigerant and water mass flux ranges, saturation temperatures. A cross flow condensation module was constructed using water as the coolant. The test section was 20cm wide, contained 10 channels, 29cm long and fabricated from copper. The water channels were fabricated from brass. Pressure drops ranged from 1 - 25 kPa for FC-72 mass flues ranging from 68 – 387 kg/m^2s. Average heat transfer coefficients ranged from 1-7 kW/m^2K for the same range of FC-72 mass fluxes. Heat transfer coefficient was shown to increase with increasing FC-72 flow rate because of increased interfacial shear leading to a thinner liquid film. As water mass flux is increased the condensation heat transfer coefficient decreased slightly however the

change was negligible compared to FC-72 flow rate. (Sung-Min Kim, Issam Mudawar. 2012)

Garimella conducted experiments to map flow regimes and determine pressure drop and heat transfer models for two-phase R134a during condensation in square, round, and rectangular horizontal micro channels. Refrigerant mass flux, inlet quality and hydraulic diameter were varied between 100-800 kg/m^{2}s, 0.0–1.0 and 1.0-4.0mm respectively. The annular regime is characterized by the uniform liquid film around the channel walls where surface tension has more of an affect of spreading the liquid to the corners. In the wavy regime gravity has a larger effect and the liquid falls to the bottom of the channel. The type of wave is determined by the interfacial shear between the liquid and vapor. Intermittent consists of plug and slug flow where large vapor bubbles flow through the liquid phase. Dispersed flow is mostly liquid with smaller bubbles entrained inside of the liquid. At low qualities < 0.1 plug and slug flow are present for all mass fluxes and as quality in increased the transition from disperse/intermittent to wavy occurs, this transition happens slightly later and low mass fluxes < 250. As mass flux and quality increase there is a transition from discrete to disperse waves. As mass flux increases this transition occurs at lower qualities because of the increase in interfacial shear. The transition from wavy to annular occurs at mass flues greater than 200 at qualities greater than 0.8. Garimella also performed condensation heat transfer experiments using HFC R134a as the working fluid over a wide range of mass fluxes, inlet quality's as well as channel hydraulic diameter. Heat transfer coefficient was shown to increase with increasing inlet quality and mass flux. A reduction in hydraulic diameter also increased heat transfer coefficient. At lower qualities the effect of hydraulic

diameter was much lower than at higher qualities. The effect of saturation pressure was not explored in this study and no pressure drop results were presented. (Srinivas Garimella, 2004)

More recently Garimella performed microchannel condensation experiments with hydraulic diameters from 100-200 μm using HFC R134a as the working fluid. Mass fluxes, saturation temperatures and average quality ranged from 300-800 kg/m^{2}s, 30-60 C and 0.2 to 0.7 respectively. Similar trends to his previous work were noted. Heat transfer coefficient and pressure drop increasing with increasing quality and mass flux and decreasing saturation temperature. Heat transfer coefficients ranged from 30 to 70 kW/m^{2}s at quality's from 0.2 to 0.65 at a mass flux of 800kg/m^{2}s at 30C saturation temperature. Pressure drops ranged from 90-220kPa for the same data points. (Agarwal A, Garimella S., 2010)

Wang and Wang conducted experiments using HFC R134a as a working fluid, measuring condensing heat transfer coefficient and pressure drop in a microchannel heat exchanger. 40 microchannels with width 0.15mm depth, 0.5mm width, 80mm length was separated in to 3.5mm branches for added enhancement. Tests were run at three different system pressures and refrigerant mass flow rates of 850kPa, 750 kPa 650 kPa and 28mg/s 43mg/s, 57mg/s respectively. Heat transfer coefficients reached 2.4 kW/m^2°K and pressure drop was 60kPa. Heat transfer coefficient and pressure drop increased with increasing refrigerant flow rates. Inlet or average quality was not varied in this study. The mass flux in these experiments is very low, around 0.01 kg/m^{2}s, which explain the lower heat transfer coefficient values. However the 80mm flow length in the

microchannel makes the pressure drop extremely high for these low mass fluxes. (Wang, W., and Wang, X, 2010)

Microchannel surfaces have the ability to increase heat transfer capability however with smaller hydraulic diameters the pressure drop penalty becomes higher. A higher number of shorter channels in parallel would yield the best results, Cetegen showed a manifold microchannel design with hydraulic diameters of 80μm that allows for a large number of microchannels in parallel. Cetegen's experiments showed heat a transfer coefficient of 200 kW/m^{2}K with a pressure drop of 60kPa at a mass flux of 1400 kg/m^{2}s using R245fa as a working fluid. Cetegen's experiments are for evaporation and in general condensation heat transfer coefficients tend to be lower than evaporation heat transfer coefficients however the same force-fed design can be adapted for condensation. (Cetegen, E., 2010) Table 1 shows a summary of the literature reviewed.

Table 1 Condensation Literature Summary

Author	Dh [mm]	G [kg/m^{2}s]	Working Fluid	T_sat [C]	x	E/C	S/M	DP [kPa]	HTC [kW/m^{2}K]
Cavallini et al 2001	8	100-750	R134a, R125, R32, R410A, R236ea	30-50	0.15-0.85	C	S	1.6-24	1.5-8.0
Wang and Wang 2010	0.23	0.0093, 0.0143, 0.0190	R134a	33.45, 29.06, 24.20	>1	C	M	25.0-60.0	0.4-2.4
Kimi, Kim, Mudawar 2012	1	68-367	FC-72	57-62	>1	C	M	1.0-25.0	12.0-1.0
Ping C, Guodong W, Xiaojun Quan 2009	0.173	175	R134a	NA	0.7	C	M	202	70
Cetegen 2010	0.08	1400	R245fa	NA	NA	E	M	60	200
Garimella 2010	0.1-0.2	300-800	R134a	30-60	0-1	C	M	20-220	20.0-70.0
Garimella 2004	1.0-4.0	200-800	R134a	NA	0-1	C	M	10-90	2-10

Liu. 2013	0.952,1.152	200-800	R152a	40,50	0.1-0.9	C	S	8.5-59.5	4-14
Al-Hajri 2013	0.7	50-500	R134a R245a	30-70	>=1	C	S	9.5-47.5	4-12
Park 2009	0.89	200-800	CO2	-15,-25	0.1-1.0	C	M	0.95-13.3	3-9

From the literature that is reviewed we can see that the parameters that have the greatest effect on condensation heat transfer coefficient are inlet quality, saturation pressure/saturation temperature, hydraulic diameter and mass flux. For this study we will investigate the effects of refrigerant mass flux, saturation temperature and inlet quality while keeping the hydraulic diameter of the channel constant. This is different than the research in literature because this many channels have not been tested at this hydraulic diameter and the manifold microgroove design has not been tested at this size and capacity for condensation. Distributing the flow over this length of microchannels has not been attempted. The next chapter will discuss the Forced design, test loop, test section, refrigerant manifolds, refrigerant and water side surfaces, the water side inserts, experimental procedure and data reduction.

Chapter 3 Experimental Setup

3.1 Force Fed Design

The force-fed manifold design allows for the heat transfer enhancement of microchannels without the large pressure drop penalty of conventional microchannels. It is able to take one long microchannel and turn it in to many smaller microchannels in parallel so that the pressure drop is reduced by 1/n where n is the number of channels in parallel. Figure 1 shows the force-fed design for condensation.

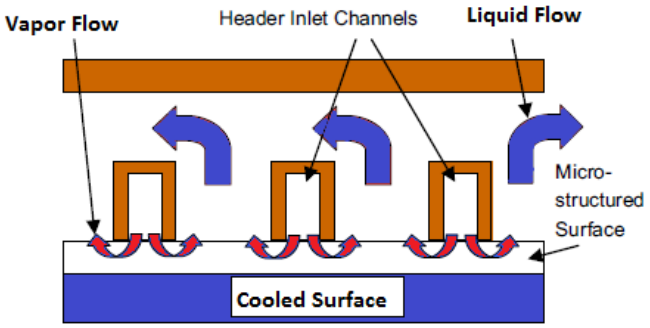

Figure 1 Forcefed Design

Vapor flows in to the vapor manifold inlets, down in to the microchannel where it condenses on the cooled surface then the liquid exits through the liquid manifold outlet. The design for this system will be an annular condenser with the microchannels on the outside of the tube and the manifold wrapped around that. The next section will explain the test loop.

3.2 Experimental Test Apparatus

Figure 2 shows a picture of the test loop including the two phase loop, data acquisition system and evaporator transformer.

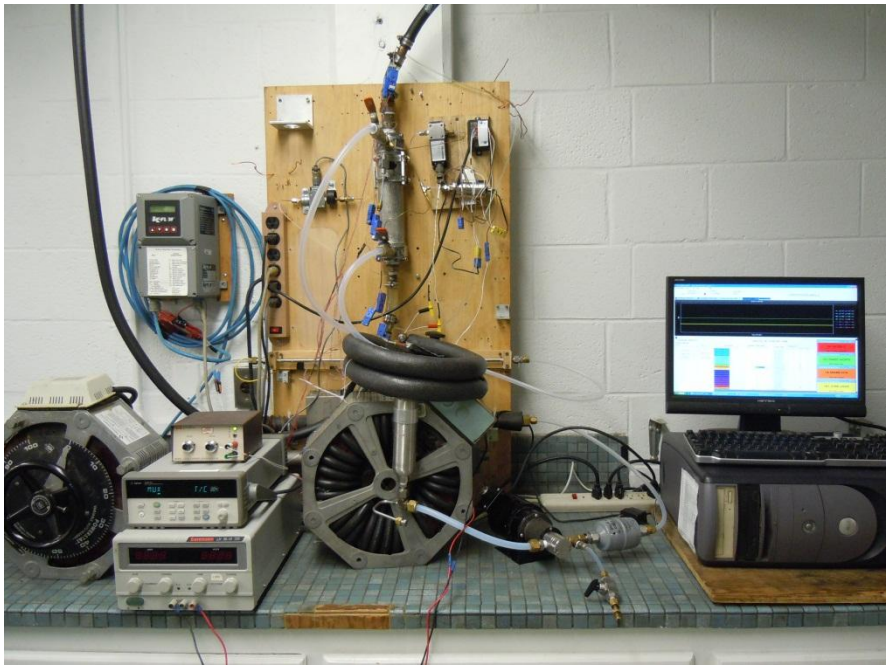

Figure 2 Picture of two phase loop for testing annular condenser

Figure 3 shows the schematic of the experimental test setup that was fabricated and assembled in order to test the heat transfer and pressure drop characteristics of the manifold microgroove condenser.

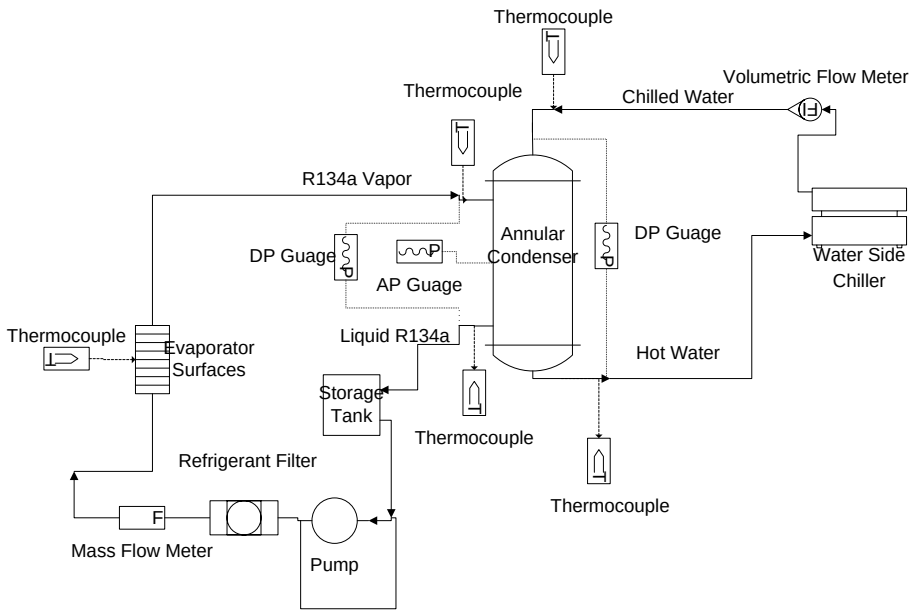

Figure 3 Schematic of two phase loop for testing of annular condenser

A Baldor Reliance DC motor pumps the liquid refrigerant from the volume chamber through the evaporator and through the test section. ABB K-flow mass flow meter measures the refrigerant mass flow rate. GPI turbine flow meter measures the water flow rate. A Cool flow HX-500 chiller removes heat from the cooling water. Rhomar Pro-tek 922 corrosion inhibitor was added in a 50:1 ratio to the cooling water to prevent corrosion on the water side of the aluminum heat exchanger tube. Addition of the inhibitor didn't affect the heat transfer properties of the water. Agilent data acquisition unit records all of the data at two second intervals. Temperature of the refrigerant and water are measured at both the inlets and outlets using four T-type thermocouples. Differential pressure between the inlet and outlet is measured on both the water and refrigerant side by Valadyne DP50 differential pressure transducers. The diaphragm in the DP50 transducer was selected so that it provided the correct range and good resolution. Absolute pressure is measured on the refrigerant side to check

saturation temperature with a Setra 280E 0-250psi absolute pressure transducer. Refrigerant flow rate was controlled using a variable DC power source. System pressure is controlled by changing the inlet temperature of the cooling water.

3.3 Working Fluids

R134a and R236fa were chosen as the working fluids for this study. One is a high pressure and one is a low pressure refrigerant. R134a is a widely used commercial refrigerant in many different areas such as refrigeration HVAC and automotive. R236fa is a newer low pressure refrigerant that is phasing out older less environmentally friendly refrigerants and is being considered for aircraft applications. Table 2 show shows the thermodynamic and physical properties of both the working fluids.

Table 2 Working Fluid Properties

	R236fa		**R134a**	
	liquid	vapor	liquid	vapor
Cp [kJ/kh-K]	1.277	0.8472	1.424	1.032
ρ [kg/m^3]	1359	18.28	1207	32.34
k [W/m-K]	0.0745	0.0042	0.08325	0.01456
P_{sat}[kPa]	272.3		665.8	
μ[kg/m-s]	0.000194		0.000306	
σ [N/m]	0.00985		0.00808	
h_{fg} [kJ/kg]	146.7		177.8	

3.4 Test Section

Figure 4 shows a picture of the condenser test section with pressure and temperature measuring instrumentation.

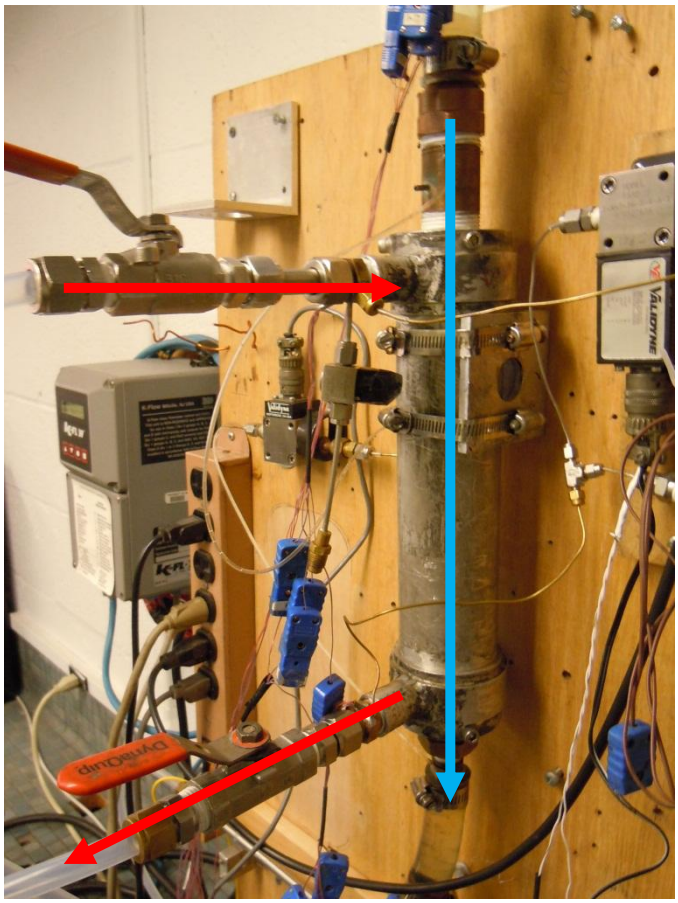

Figure 4 Condenser Test Section

Water flows from top to bottom along the axis of the annular condenser. T type thermocouples measure the temperature of the inlet and outlet and pressure drop is measured across the water side of the condenser. Refrigerant vapor leaves the heater and enters the test section at the top, is condensed in the test section and the liquid refrigerant leaves the bottom of the test section. Temperature is measured at the inlet and outlet of the condenser. Absolute pressure is measured at the outlet of the condenser. The next section will discuss the two different refrigerant manifolds that were tested.

3.4.1 Refrigerant Manifold

Two different refrigerant manifolds were fabricated from Teflon sheets for testing. The Teflon sheet was glued to a metal base for securing during fabrication then a

slitting saw was used the machine the manifold channels. When fabrication was complete the channels were cleared of debris and excess Teflon and the manifold was removed from the base using acetone. Both manifolds are shown in Figure 5.

Refrigerant Manifold A 1mm x 1mm channels and 1.5 mm flow length

Refrigerant Manifold B 2 x 2 mm channels, 3mm flow length

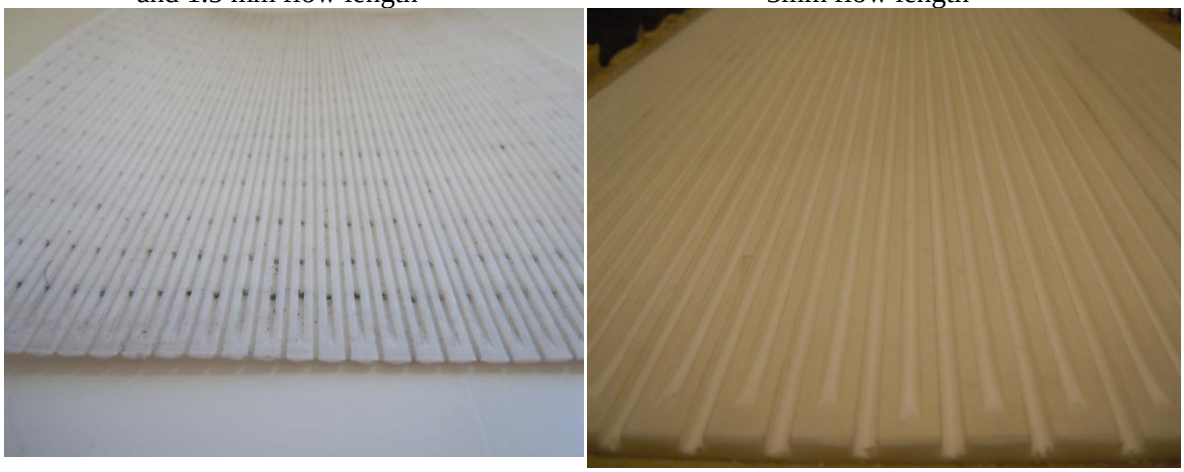

Figure 5 Refrigerant Manifolds

Refrigerant manifold A has 32 pairs of inlet and outlet channels that are 1mm x 1mm and a flow length in the microchannel of 1.5mm. Refrigerant manifold B has 16 pairs of inlet and outlet channels that are 2mm x 2mm and a flow length of 3mm. Table 3 summarizes the refrigerant manifold geometry.

Table 3 Refrigerant Manifold Geometry

	Flow Length	**Vapor Channel**	**Liquid Channel**
Manifold A	1.5mm	1mm x 1mm	1mm x 1mm
Manifold B	3mm	2mm x 2mm	2mm x 2mm

The next section shows the refrigerant and water side surfaces.

3.4.2 Microgroove Tube

Microgroove tubes were fabricated by Wolverine using their micro-deformation technique. The finished product is shown in Figure 6

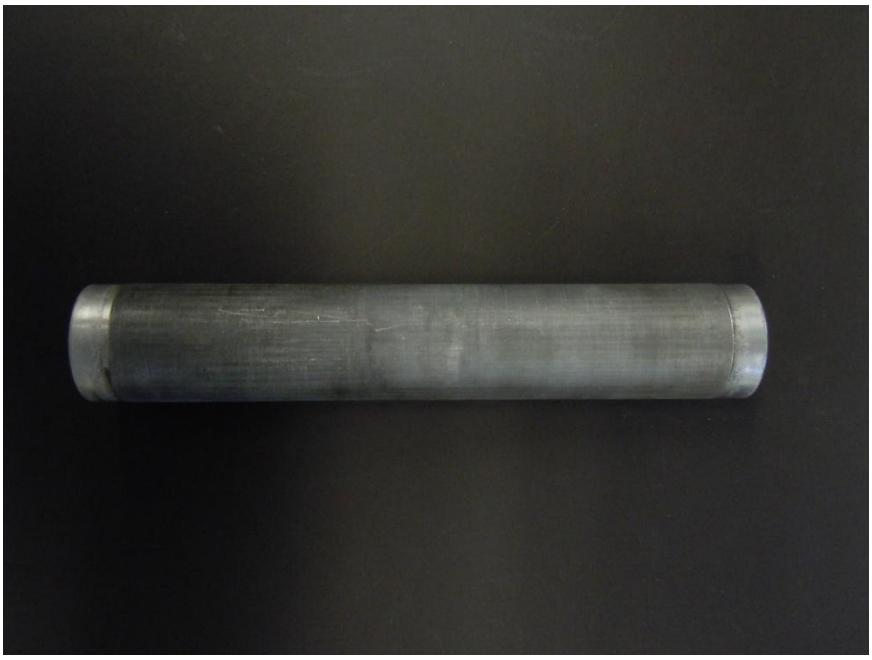

Figure 6 Microgroove tube

Figure 7 shows the microgrooves on the refrigerant side and the mini channels on the water side. The micro grooves are 60 x 600 μm and the mini channels are 800 x 1400 μm.

Refrigerant Side Microgrooves Water Side Minichannels

Figure 7 Refrigerant and Water Side Surfaces

3.4.3 Water Side Header

The water side header was fabricated from PVC pipe, Delrin rods and steel rods. First the PVC was milled down to the desired diameter. Then then ends were plugged with the Delrin rods. Holes were drilled through the PVC and Delrin along the rim and the steel rods were inserted. The steel rods were bent up and tied together with wire, which served to keep the insert in the middle of the tube and stop it from blocking the exit. The water side insert is shown in Figure 8.

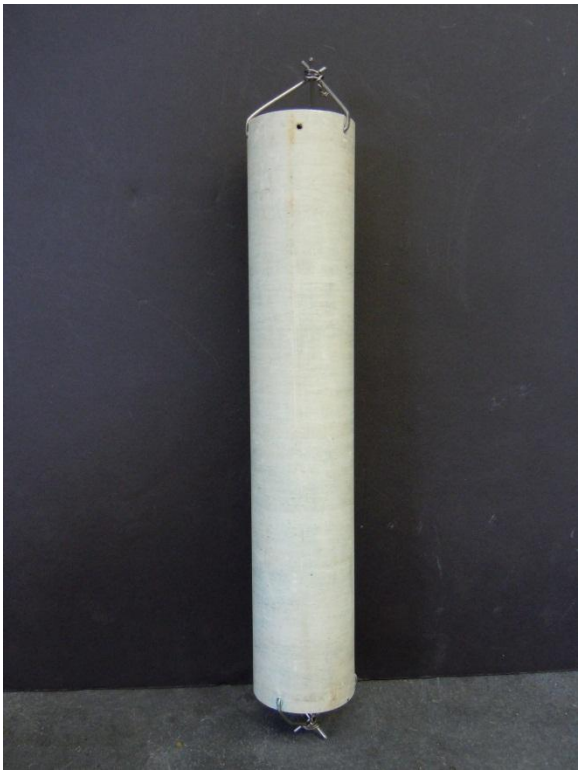

Figure 8 Water Side Header

The next section will describe how the condenser was assembled for testing

3.5 Assembly

To assemble the condenser first all the parts were cleaned of any debris and oil with hexane and a soft brush. Next the manifold was wrapped around the microgroove tube and secured using clear nylon line. This ensures that the manifold is tight around the microgrooves and the vapor will be forced in to the microgrooves. Any gaps created by the manifold being not long enough to wrap around the tube were filled in with Teflon tape. After this the liquid vapor seal is installed which forces the vapor in to the manifold and prevents it from going directly to the liquid outlet, this is done differently for each manifold. Manifold A was sealed suing an aluminum ring around the outside of the manifold and an O-ring to seal it against the condenser casing. Manifold B is thicker

than manifold A and the aluminum ring would not fit and couldn't be milled down. The solution was to use copper wire to create a metal ring by wrapping it around the outside of the manifold and soldering it in place. This was done twice to create two metal rings so that the O-rings would fit in between them and not move when the tube was inserted in to the casing. Figure 9 shows the liquid vapor seal and the nylon line on the outside of the manifold.

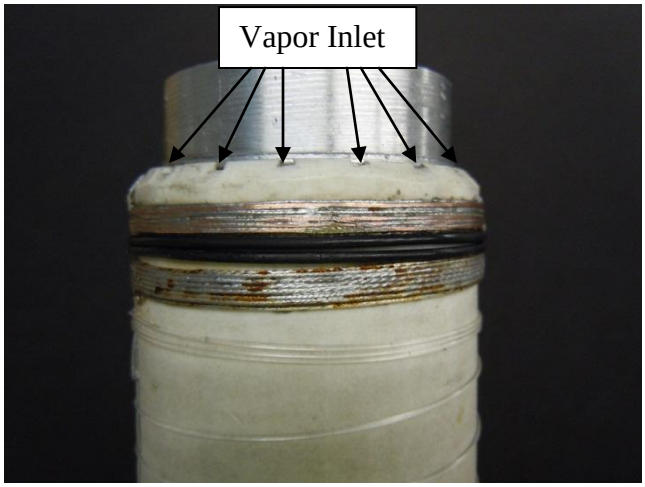

Figure 9 Liquid Vapor Seal

After the liquid vapor seal is installed the O-rings are lubricated with vacuum grease and the tube is inserted in to the casing. The refrigerant water seals are inserted in to the casing on either end and the water side caps are installed. The next section will explain the experimental procedure.

3.6 Experimental Procedure

The entire loop was first vacuumed and leak checked for 6 min. If the leak rate was lower than 2 Pa/sec then the system was ready to charge with refrigerant. The system was first charged with 600g of refrigerant and the charge level was adjusted so that the proper range of mass flow rates was achieved. When running experiments first

the DAQ system was started then cooling water was turned on followed by the refrigerant pump and the heater. The water temperature was adjusted until the system was at the proper pressure then the pump power was adjusted until the correct mass flow rate was achieved then we wait 2-3 minutes so that the system is at steady state. Data was taken for 2 minutes and at any point if the data became erratic then the process was restarted and repeated until steady state was reached. After data was taken the heater and water temperature was adjusted. After the system came to steady state the flow rate was adjusted if it had changed and the process was repeated for all data points. 'The range of test parameters, quality, saturation temperature, and mass flow rates, were 0-1.0, 26-34C and .007-.024 kg/s. For manifold B refrigerant mass flux, saturation temperature and inlet quality were varied and only refrigerant mass flux and inlet quality were varied for manifold A. The next section will explain the data analysis and calculations.

3.7 Data Reduction

Determining heat transfer coefficient requires knowing the surface temperature on the heat exchanger tube as well as the temperature of the fluid in the flow. The design of the heat exchanger does not allow monitoring of the surface temperature and placing temperature sensors in the channels is not feasible as it will disrupt the flow and influence the measurements significantly. The other option is to use a thermal resistance network and find the refrigerant side heat transfer coefficient from the individual resistances and the overall resistance. Figure 10 shows the thermal resistance network.

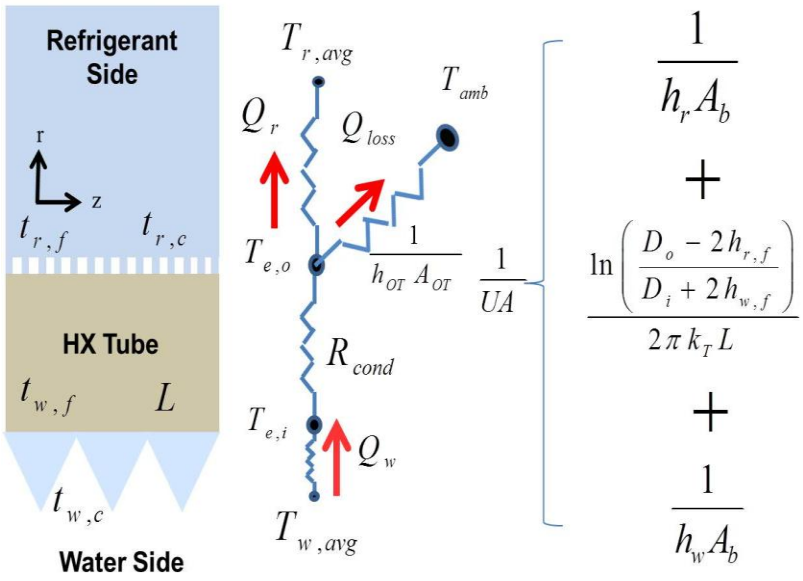

Figure 10 Condenser Thermal Resistance Network

The overall resistance is made up of the refrigerant side, water side and the conduction resistance through the tube. Since most of the experiments were conducted at or near room temperature and the outside heat transfer coefficient was low the heat losses were assumed to be negligible. The conduction resistance is known from the dimensions of the tube and the properties of the material. Calculating the overall resistance and the water side resistance will allow us to solve of the refrigerant side heat transfer coefficient. We can determine the overall heat transfer coefficient from the cooling capacity and LMTD given in Equations 1 and 2.

$$Q = \dot{m}_{water} \times C_{p\,water} \times \left(T_{w,\ out} - T_{w,\ in}\right) \qquad (1)$$

$$LMTD = \frac{T_{w,\ out} - T_{w,\ in}}{\ln\frac{T_{w,in} - T_{sat}}{T_{w,\ out} - T_{sat}}} \qquad (2)$$

Equations 3 and 4 show the calculation for overall heat transfer coefficient and refrigerant side heat transfer coefficient respectively.

$$U = \frac{Q}{A \times LMTD} \quad (3)$$

$$\frac{1}{U \times A} = \frac{1}{h_{ref} \times A} + \frac{1}{h_w \times A} + R_{cond} \quad (4)$$

In order to determine the refrigerant side heat transfer coefficient we also must know the water side heat transfer coefficient. A correlation for the water side heat transfer coefficient was determined by the Wilson Plot method where the refrigerant side properties, pressure, flow rate, quality, which determine the refrigerant side heat transfer coefficient are kept constant and the water side flow rate is changed. Since the water side is in single phase the heat transfer coefficient is only a function of Reynolds number or water velocity. [8] We can take $h_w = C/V^n_{water}$ then Equation 3 becomes

$$\frac{1}{U} = K + C\frac{1}{V^n} \quad (5)$$

K is a constant representing refrigerant side heat transfer coefficient and the conduction resistance. Data was taken at water flow rates for the range of 0.1893 to 0.5679 L/s and the data was fitted to equation 5 and the constants *C* and *K* were found for various values of n. The least squares regression was minimized to get the final values of *C* and *n* where found to be $n = 0.754$ and $C = 0.0001185$. h_w vs water flow rate is graphed in Figure 11**Error! Reference source not found.** and has a range of 7,000 to 17,000 W/m^{2}K.

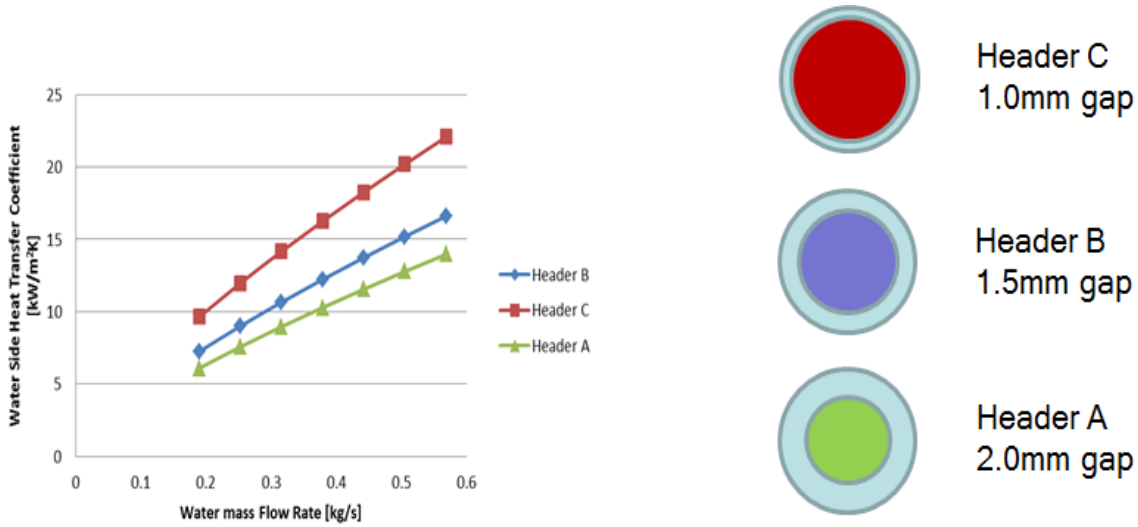

Figure 11 Variation of waterside heat transfer coefficient versus water mass flow rate for different waterside headers

Quality is calculated based on the condenser cooling load, refrigerant mass flow rate and condenser outlet conditions. The first step is to calculate the refrigerant enthalpy at the outlet of the condenser. This is calculated using the pressure and temperature at the outlet of the condenser because the refrigerant exits subcooled. Next the enthalpy at the inlet of the condenser is calculated using the cooling load of the condenser and mass flow rate.

$$Q = \dot{m_{ref}} \times (h_{in} - h_{out}) \qquad (6)$$

When we know h_{in} we can back calculate for the quality using the system pressure. Pumping power was calculated using equation 7, the pressure drop across the condenser, the refrigerant mass flow rate and the refrigerant liquid density.

$$W_{pump} = \frac{\dot{m_{ref}}}{\rho_{ref}} \times DP_{cond} \qquad (7)$$

Now that we know the pumping power we can calculate the COP of the heat exchanger using equation 8.

$$COP = \frac{Q_{cond}}{W_{pump}} \qquad (8)$$

This is only one way we calculate COP. Later when comparing our condenser to literature we will use COP calculated in equation 9

$$COP = \frac{Q_{cond}}{W_{pump} \times LMTD} = \frac{h_{ref} \times A_{HT}}{W_{pump}}$$

All uncertainty calculations were performed in EES (Engineering Equation Solver) using the uncertainty propagation tool.

Parameter	**Uncertainty**
Temperature	0.05C
Pressure	3kPa
Refrigerant Mass flow rate	.01 g/s
Water Mass flow rate	.005 gal/min
h_water	500 W/m^{2}K

Chapter 4: Experimental Results

In this chapter the experimental results using both refrigerants and manifolds is presented and analyzed.

4.1 Initial Experiments

The first manifold that was tested was manifold B using R134a as the working fluid. The effect of mass flow rate, saturation temperature and inlet quality was tested. Mass flow rates were ranged from, 7-23 g/s. Saturation temperature was tested at 26C and 34C and inlet qualities were changed from 0 to 1. Figure 12 shows the effect of saturation temperature.

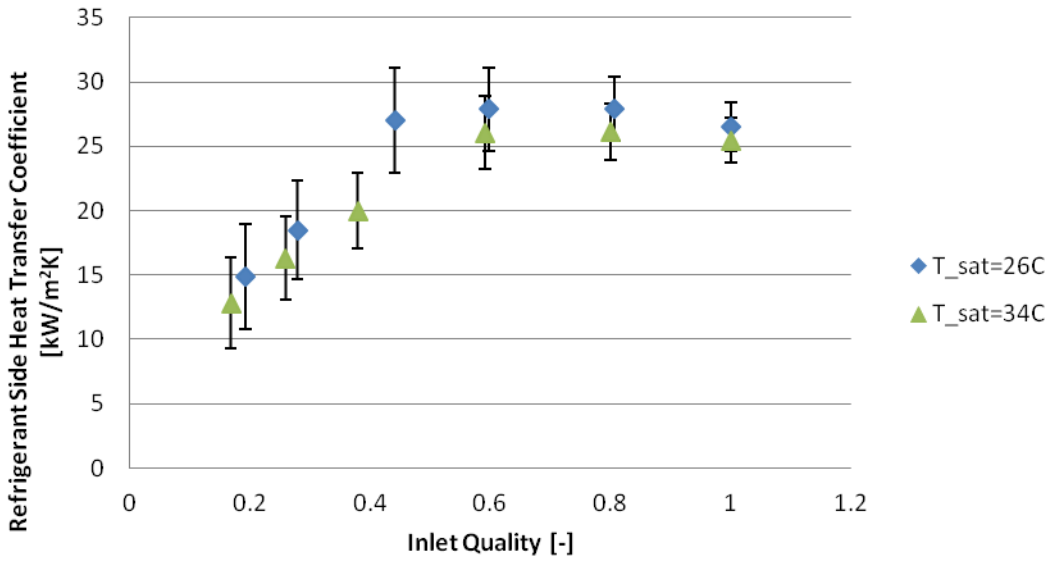

Figure 12 Variation of refrigerant side heat transfer coefficient with inlet quality for different saturation temperatures (Refrigerant: R134a, Manifold: B)

These tests were run at mass flow rates of 0.015 kg/s which is a microchannel mass flux of 6.25 kg/m^2-s and manifold mass flux of 234 kg/m^2-s. As saturation temperature is decreased the condenser pressure decreases which decreases the refrigerant vapor density. The decrease in density increases the volumetric flow rate in order to keep the mass flow rate constant. This increase in volumetric flow rate enhances the effects of convection which raises the heat transfer coefficient. The effect is more prominent as inlet quality goes from 0 to 0.5 but the effect decreases as quality goes from 0.5 to 1. This might be due to flow distribution in the manifold changing with the inlet quality. Figure 13 shows the effect of microchannels mass flux for the entire range of inlet qualities and T_sat=30C.

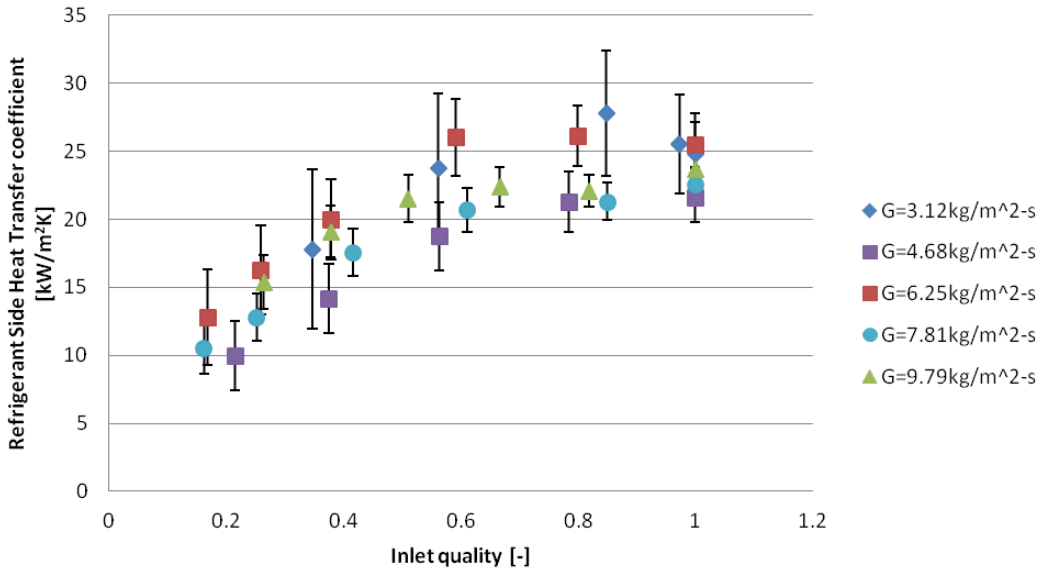

Figure 13 Variation of refrigerant side heat transfer coefficient with inlet quality for different microchannel mass fluxes (Refrigerant R134a, Manifold: B, T_sat=30C)

Heat transfer coefficient increases with increasing inlet quality and starts to level off near inlet qualities of 0.7. As the amount of vapor increases the thinner the liquid

film in the microchannel and the lower the thermal resistance will be creating higher heat transfer rates. The heat transfer enhancement should be seen all the way up to qualities of 1 however it is possible that the flow distribution is changing as the inlet quality is changing. It should be noted that the experimental data uses inlet quality compared to literature where the average quality is used. As average quality approaches 1 the heat transfer should decrease because no phase change takes place. There is not much difference between the heat transfer performances for different mass fluxes because at such mass flux flow is highly laminar. Figure 14 show the variation of pressure drop with inlet quality and microchannel mass flux

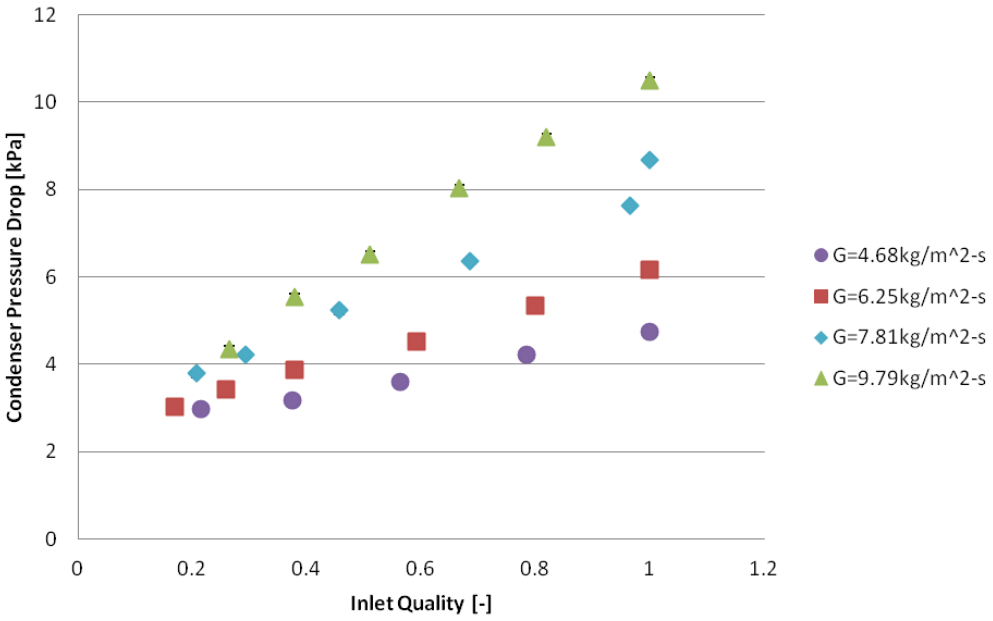

Figure 14 Variation of condenser pressure drop with inlet quality showing effect of microchannel mass flux, T_sat=30C

Pressure drop increases with increase in inlet quality and increasing microchannel mass flux. As the inlet quality increases the volume flow rate increases which lead to the increase in pressure drop. In addition the vapor velocity is about 20 times higher than the

liquid velocity which also leads to higher pressure drops. The pressure drop also increases with increasing microchannel mass flux and the percent increase in pressure drop increases as inlet quality increases. Compared to heat transfer coefficient, pressure drop shows more sensitivity to microchannel mass flux. This increase in sensitivity is dbecause most of the pressure drop occurs in the manifold. Table 4 shows the manifold mass flux for the mass flow rates tested for manifold B.

Table 4 Manifold B mass flux for tested mass flow rates

mass flow rate [g/s]	G_man[kg/m^2-s]
7.5	117.1875
11.25	175.78125
15	234.375
18.75	292.96875
23.5	367.1875

As seen, the mass fluxes in manifold are much higher than the microchannel mass fluxes because the manifold area is much smaller than the collective microchannels area. The combination of low manifold area and high manifold mass flux lead to the manifold contributing a large portion of the condenser pressure drop. Table 5 shows the comparison between the manifold and microchannel areas for both manifold designs.

Table 5 Manifold and Microchannel area comparison

	Manifold A	**Manifold B**
Micro-channels Collective Area [m^2]	$9.6\ 10^{-3}$	$4.8\ 10^{-3}$
Manifold Area [m^2]	$32\ 10^{-6}$	$64\ 10^{-6}$
A_{mchn}/A_{man}	150	75
Manifold Vapor Velocity [m/s]	12	6

Calculations were done at a mass flow rate of 15g/s and saturation temperature of 30C. The microchannel collective area is much greater than the manifold area for both manifolds. This leads to a majority of the pressure drop being in the manifold which has a large effect on the flow distribution. Manifold A was not tested over the whole ranges of saturation temperatures and mass fluxes because they were shown not to have a very

large effect on Manifold B. Since inlet quality has the most effect on pressure drop and heat transfer coefficient that will be the parameter varied in the tests using R236fa and manifold B and both refrigerants with Manifold A. In the next section we will compare the two different manifold and refrigerants.

4.2 Manifold and Refrigerant Comparison

Both manifolds were tested using both R134a and R236fa as the working fluids. Both manifolds were tested at mass flow rates of 15g/s, T_Sat 30C and through the full range of inlet qualities. Figure 15 and Figure 16 shows the variation of heat transfer coefficient and pressure drop for both manifolds and refrigerants as inlet quality is changed.

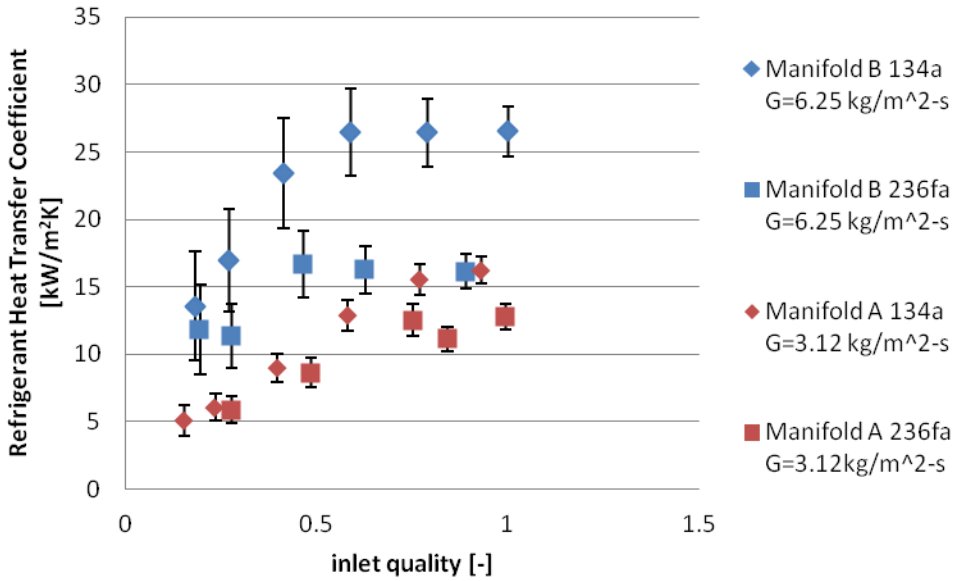

Figure 15 Variation of refrigerant heat transfer coefficient with inlet quality showing effect of manifold geometry and working fluid

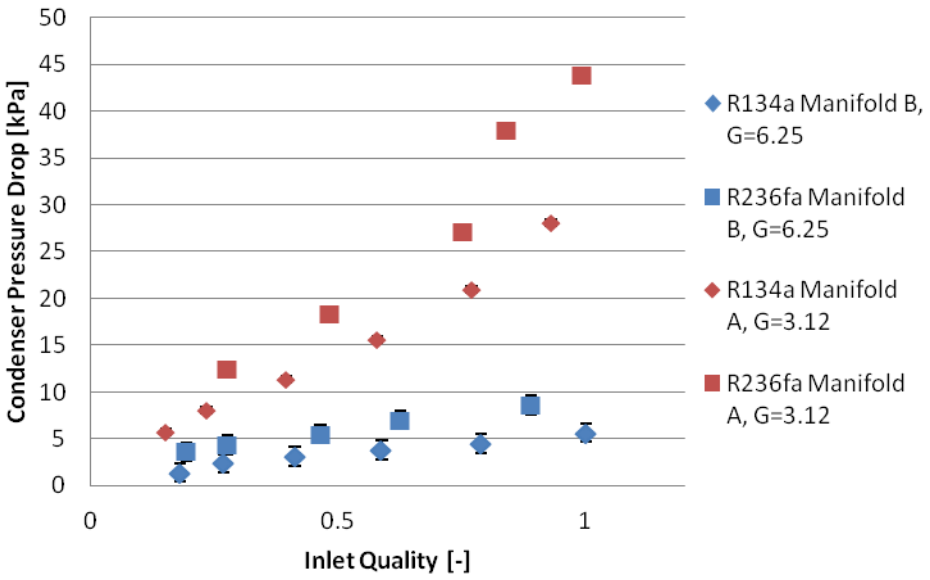

Figure 16 Variation of condenser pressure drop with inlet quality showing effect of manifold geometry and working fluid

Manifold B has better heat transfer and pressure drop performance for both R134a and R236fa as working fluids. The increase in manifold area decreases the pressure drop as well as changes the flow distribution in the microchannels. R134a has slightly better heat transfer and pressure drop performance than R236fa for both manifold A and manifold B because the vapor density of R236fa is less than R134a which increases the volumetric flow rate of the vapor leading to higher pressure drops. This should also enhance the heat transfer performance however the increase in pressure drop causes maldistribution of the flow which decreases the heat transfer performance. Seeing that the manifold has a significant pressure drop and has a large effect on the heat transfer and pressure drop, a pressure model was created to look at the flow distribution in the manifold and microchannels and see if there are any issues.

4.3 Manifold Flow Model

A manifold flow model was created to look at the flow distribution in the manifold and microchannels. Certain assumptions were made in order to make this model. First the model does not take in to account any heat transfer and only predicts the local pressure in the manifold and microchannels. Second the pressure drop in the microchannel was set to change linearly with velocity. The third is that the inlet to the manifold is pure vapor, x=1, and the outlet to the manifold is pure liquid, x=0. (R. Mandel, 2013). The domain of the model is one pair of inlet and outlet channels and the microchannels as shown in Figure 17.

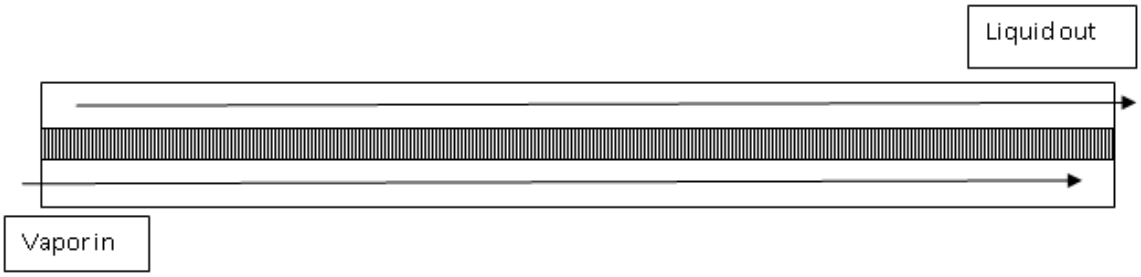

Figure 17 Manifold microchannel pressure model domain

Inputs to the model are the manifold length width and height, inlet vapor velocity, working fluid, and temperature. Mass and momentum balance are used in order to get the pressure at all points on the manifold. Beta is the parameter that determines the amount of flow maldistribution is the difference between the minimum and maximum pressure divided by the median pressure. The model was run using a mass flow rate of 15g/s, R134a as the working fluid and 30C temperature. Manifold A and B were tested for these conditions. Figure 18 and Figure 19 show the model results for both manifolds. The green line is the relative pressure in the manifold vapor channel, the blue line is the pressure in the manifold liquid channel and the black line is the microchannel pressure.

The vertical axis is the pressure in Pa and the horizontal axis is the length in the manifold. The vapor inlet is at x=0m and liquid outlet is at x=0.25m.

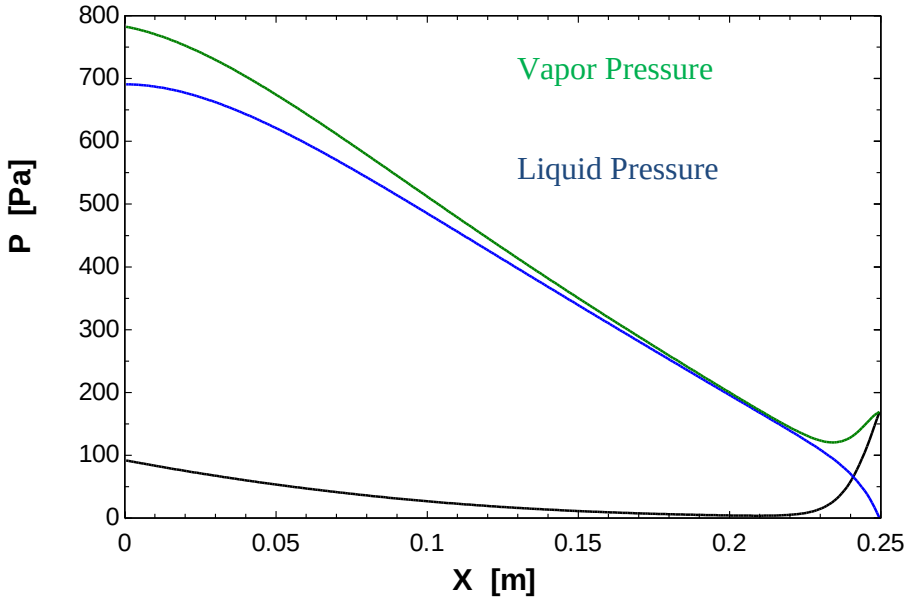

Figure 18 Manifold pressure model results Manifold A

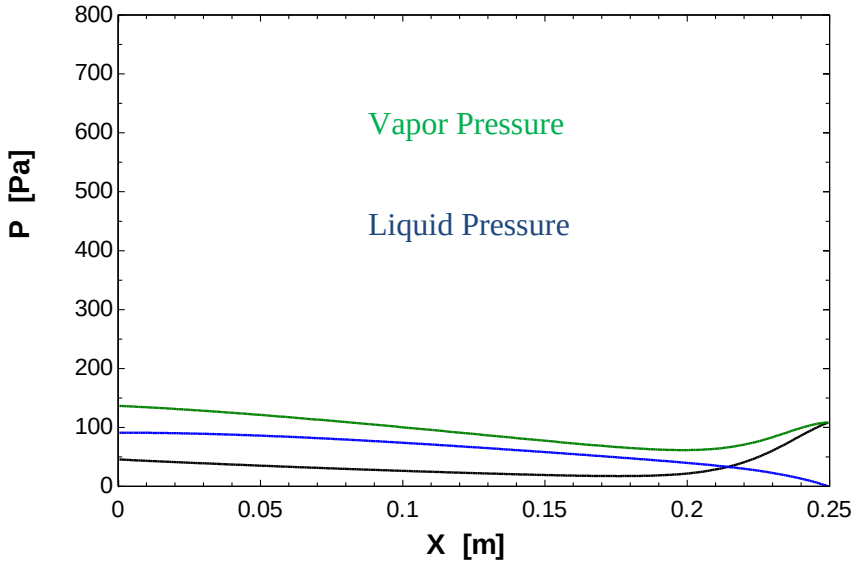

Figure 19 Manifold pressure model results Manifold B

The beta values for Figure 17 and Figure 18 are 451% and 270% respectively. The pressure drop for both graphs is on the order of a few hundred Pa where as the experimental data shows there are several kPa of pressure drop. This is because the

model only considers one pair of manifold channels. For both manifold A and B the majority of the pressure drop is in the manifold channels and the majority of the pressure drop in the microchannels is in at the end of the vapor channel. This large pressure drop at the end of the microchannel indicates that a majority of the flow is bypassing the channels and the beginning of the manifold and mostly entering the channels at the end of the manifold. Manifold B has a lower pressure drop due to the higher manifold area compared to Manifold A and therefore has better flow distribution in the microchannels. This is shown in Figure 18 and Figure 19 where the microchannel pressure on Manifold B has a majority of the pressure drop occurring from 0.20m to 0.25m whereas the majority of the pressure drop for manifold A occurs from 0.22m to 0.25m. Table 6 shows how beta varies as mass flow rate is changed for both manifold A and B.

Table 6 Variation of Beta versus refrigerant mass flow rate for both manifolds

	Manifold A		Manifold B	
mass flow rate [g/s]	V_man	Beta [%]	V_man	Beta [%]
7.5	6.009	390.8	3.004	156.9
11.25	9.014	419.1	4.507	209.7
15	12.019	451.6	6.009	270.4
18.75	15.024	558.4	7.512	340.7
23.5	18.830	635.4	9.415	446.3

As mass flow rate is increased the vapor velocity is increased which increases the pressure drop in the manifold and increases beta creating poor flow distribution. For a given mass flow rate the effect of manifold length was looked in to. Mass flow rate was set to 15g/s for manifold A and the length was changed from 0.25m to 0.05m. Figure 20 shows the variation of beta with manifold length

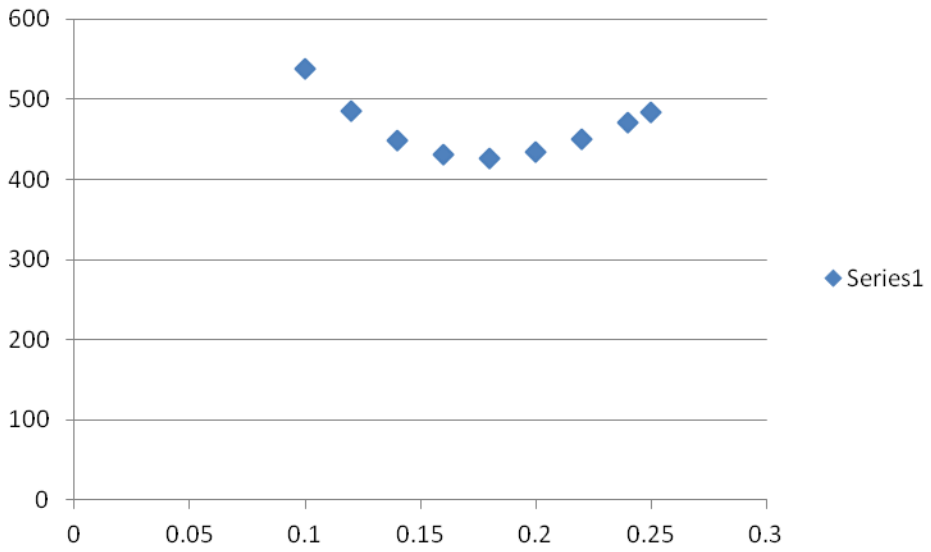

Figure 20 Variation of Beta versus manifold length

There is an optimal manifold length for this mass flow rate where the flow distribution is the best. The optimal flow length will be where the frictional and inertia pressure terms cancel each other out. The current design is the data point at L=0.25m giving a beta of 500% for manifold A at a refrigerant flow rate of 15g/s. This optimal length will be different for each mass flow rate and each manifold. This model has provided some insight in to what is going on as far as flow distribution however we would like to check to make sure the results are correct. In the next section the results from a set of experiments to validate the models predictions are presented.

4.4 Wilson Plot Experiments

If the flow is evenly distributed then the entire heat exchanger is being used properly. This is one of the assumptions made when using the Wilson plot method to calculate the waterside heat transfer coefficient correlation that was described earlier otherwise the heat transfer area is not known. If the flow is not evenly distributed then the water side heat transfer coefficient would seem smaller than it actually is due to only

part of the heat exchanger area being used. Figure 21 shows what the flow distribution could look like if the flow is not evenly distributed.

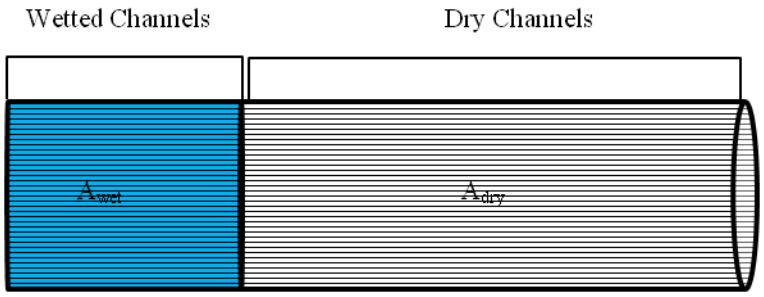

Figure 21 Possible flow distribution

If this is the case then the thermal resistance equation would change to the equation below.

$$\frac{1}{U \times A_{total}} = \left(\left(\frac{1}{A_{wet}} \left(\frac{1}{h_{cond}} + \frac{1}{h_{water}} + \frac{1}{h_{ref,wet}} \right) \right)^{-1} + \left(\frac{1}{A_{dry}} \left(\frac{1}{h_{cond}} + \frac{1}{h_{water}} + \frac{1}{h_{ref,dry}} \right) \right)^{-1} \right)^{-1}$$

Now there are two thermal resistances in parallel, wetted and dry, that makes up the overall resistance. h_{cond} will stay the same regardless of the flow distribution. If the entire waterside is not used and only a portion of it is actually transferring heat then the water side heat transfer coefficient will appear to be lower than it actually is because the area used in calculations is higher than it should be. The easiest way to test this is to reduce the heat transfer area and see if the water side correlation changes. Three more sets of reduced or altered area tests were run and the Wilson plot was repeated for each test. Figure 22 shows the manifold setup for the reduced HX area tests.

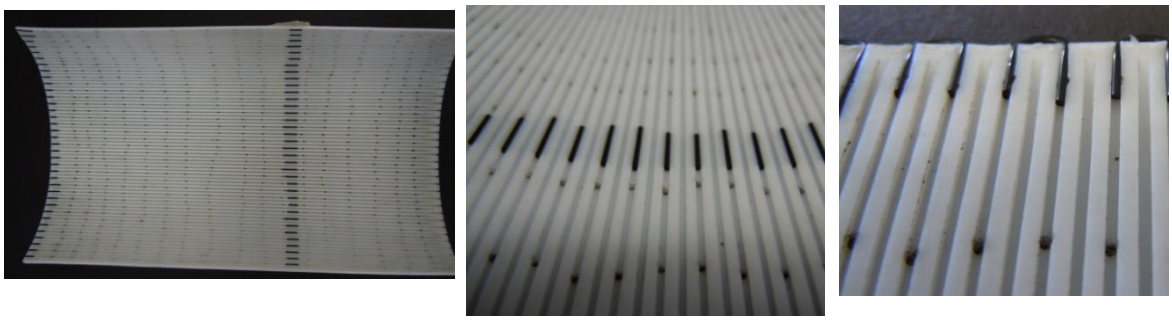

a) Entire Manifold A with 1/3 area configuration

b) Vapor channel plugs

c) Vapor channel inlet blocks

Figure 22 Reduced HX area manifold

Pieces of neoprene O-rings were placed in the manifold channel inlets to prevent vapor from entering the first part of the condenser. Additional pieces of O-rings were placed lower down the vapor channel so that the area below them would be the only area used. We had to slightly change the way the vapor was fed since making a shorter tube with a shorter manifold was not feasible. Ports were drilled every 1" all the way down the vapor channel so that the vapor can enter through them and distribute more evenly. The holes that were not used were covered with Teflon tape so that no refrigerant vapor could enter. In order to change the area the useful HX area the pieces of O-ring shown in Figure 22b were moved higher or lower depending on the value desired.

For each test the Wilson plot was repeated ranging the waterside mass flow rate values from 0.1-0.5kg/s and 1 set of heat transfer data was taken. Figure 23 shows the Wilson plot results for all of the reduced area tests compared to the original Wilson plot.

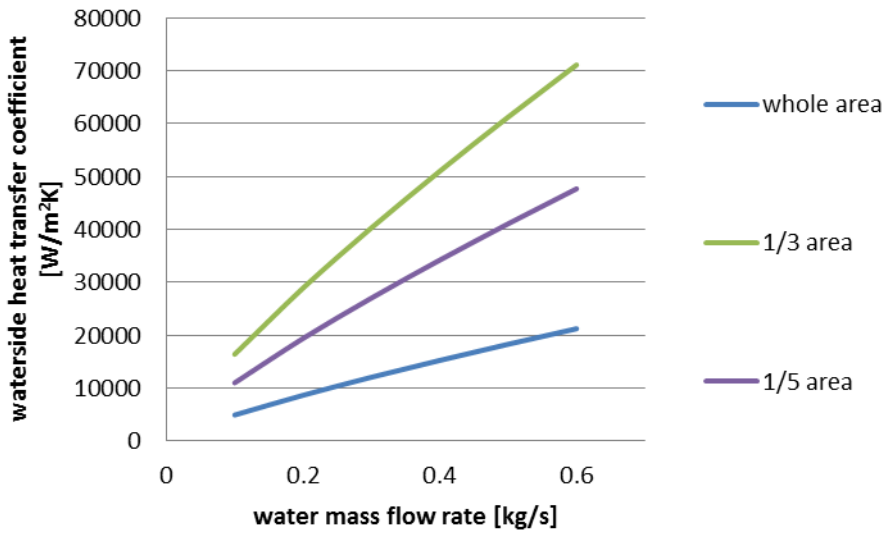

Figure 23 Water side heat transfer coefficient vs waster mass flow rate for reduced HX area tests

The waterside correlation obtained from the repeated Wilson plot experiments is different than the original Wilson plot. The 1/3 area has the highest water side correlation slope. 1/5 area has a lower correlation slope than 1/3 but higher than either of the whole area tests. This is due to 1/5 area being lower than the optimal length for this manifold and this mass flow rate making the flow distribution worse than the 1/3 area. Determining the optimal area for this test would have to be experimental as the manifold model does not simulate the way the vapor was fed in these tests. The Wilson plot results supports the results of the model and show that there are flow distribution issues in the manifold due to high pressure drops. Figure 24 shows the comparison between the whole area results presented in 4.2.

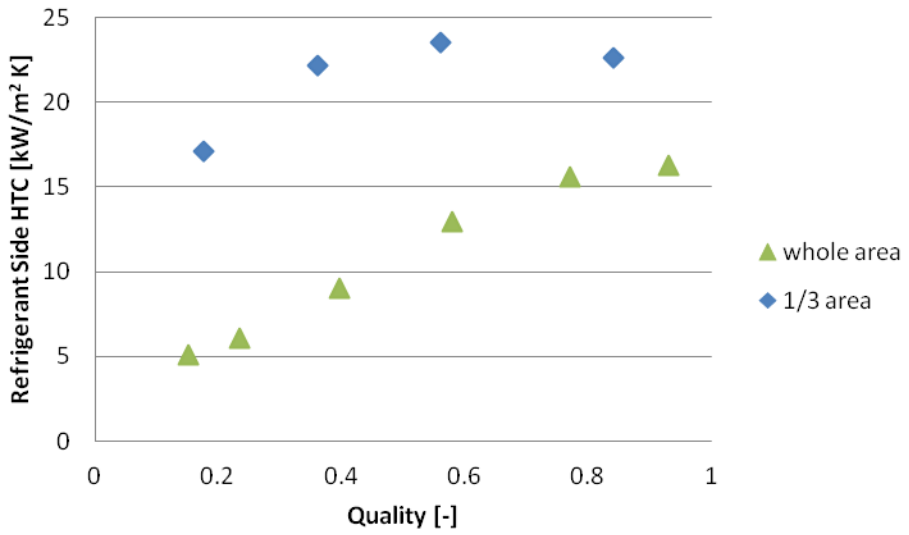

Figure 24 Refrigerant side heat transfer coefficient vs inlet quality, 15g/s T_sat=30C

The reduced area tests have much higher heat transfer coefficient than the tests utilizing the whole area. The flow distribution for the 1/3 area tests is much better that the whole area tests so the heat transfer performance is higher. The next section will compare the condenser performance to some found in literature and commercial condensers.

4.5 Condenser Comparison

In order to see how the manifold microgroove condenser performs the experimental results have been compared to commercial shell and tube condensers from Trane and Alfa Laval. The train condensers are CHX and AHX series and the Alfa Laval condensers are the CDEW-E series. Both operate using fresh water as the coolant and refrigerant as the working fluid. In order to make a fair comparison to larger capacity condensers the following metrics will be used.

$$F_1 = \frac{COP}{dT_{in}} = \frac{Q_{cond}}{W_{pump} \times dT_{in}}$$

$$F_2 = \frac{Q_{cond}}{m_{cond} \times dT_{in}}$$

F1 is the COP of the condenser divided by the difference in refrigerant and water inlet temperatures. The pumping power is the combined water and refrigerant side pumping power. This is a measure of how efficient the condenser is both thermally and in terms of pumping power. F2 is a measure of the capacity of the condenser verses the size and weight. Figure 25 shows the comparison between the Trane and Alfa Laval shell and tube condensers and the force-fed manifold condenser.

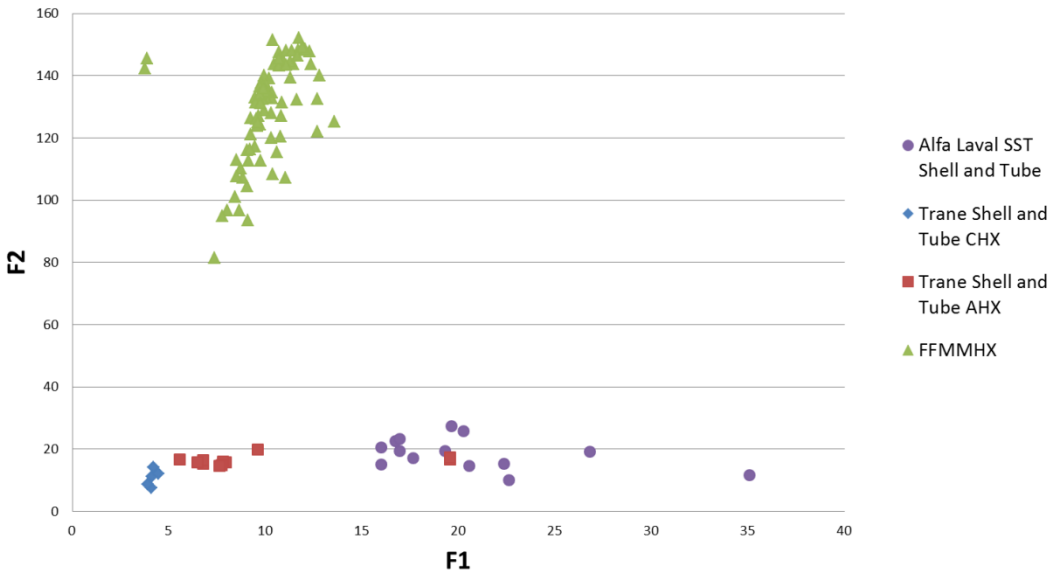

Figure 25 Commercial Condenser Comparison

When compared to commercial shell and tube condensers the FFMM condenser is comparable in the thermal and power efficiency metric and is much better in the capacity and weight metric. Refrigerant pumping power was not able to be obtained for the commercial condensers and the pumping power only consists of the water side. If the refrigerant side pumping power was included then the COP would be lower and F1 would be lower making the performance of the commercial condensers worse. The force-fed

design allows for much lower weights for a given capacity because the microgrooves add surface area and heat transfer enhancement without adding considerable volume or weight. The COP of the manifold microgroove condenser can be improved my optimizing the manifold design, this would have two effects. First is that it would reduce the pressure drop in the manifold lowering the pumping power on the refrigerant side. Second is that lowering the pressure drop in the manifold will help to decrease the flow maldistribution which will increase the capacity and effectiveness of the condenser.

Chapter 5: Air Side Optimization

5.1 Introduction

In majority of applications ultimate heat sink is air and coupling of condenser is air is essential particularly for airspace application where compact condenser is at premium interest. An optimization study for the air side of a high performance manifold microgrooved surface heat exchanger that most likely will be coupled with manifold microchannel condenser in airspace application has been performed. Unfortunately at current stage CFD techniques do not provide sufficient accuracy to perform optimization of condenser. However some conclusions extracted from single phase air side optimization could be used in condenser design. The goal of the study was to find a set of geometrical parameters that would maximize the total heat transferred and minimize the pumping power and volume. This was done by taking these three parameters and turning them in to two new parameters, heat transfer density (Q/V/dT) and pumping power density (P/V). The geometrical parameters that we changed were microchannel height, microchannel width, manifold inlet, manifold height, manifold inlet, the number of microchannels per pass, aspect ratio alpha (alpha = microchannel width/ fin thickness) and the Reynolds number in the manifold. Figure 26 shows the manifold microgroove geometry and the parameters that we chose to change.

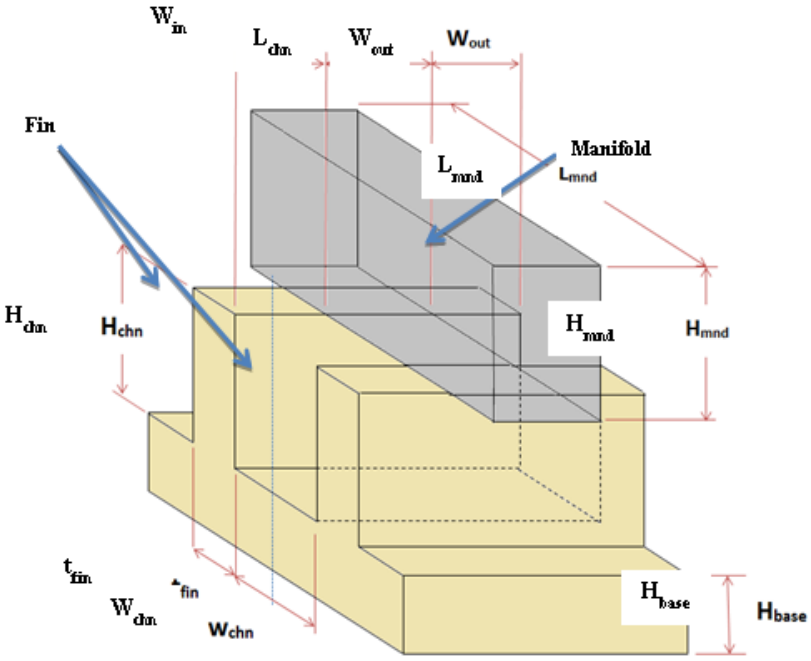

Figure 26 Manifold Microgroove Geometry

Table 7 Manifold Microgroove Geometry

Dimension	**Symbol**
Manifld Reynolds Number	Re
Manifold Length	L_mnd
Manifold Height	H_mnd
Manifold Width	W_mnd
Manifold Channel Width	W_mnd_chn
Microchannel Inlet Width	W_in
Microchannel Outlet Width	W_out
Microchannel Width	W_chn
Microchannel Height	H_chn
Microchannel Length	L_chn
Fin Thickness	t_fin
Pumping Power Density	P/V
Heat Transfer Density	Q/VdT
Flow Maldistribution Factor	F
Number of Microchannels	n
W_in=W_out	
L_chn=Wman	
aplh=Wch/tfin	

Table 7 explains the symbols that are used through the study for each part of the geometry as well as some of the assumptions that we have made. The following sections will describe the optimization methods, computational domain, parametric study, and the optimization results for this study.

5.2 Optimization Method

There are a lot of different geometries and flow rates that need to be tested in order to carry out the optimization study. Modeling the whole set of microchanels with the manifold is unfeasible due to the large amount of computing power and computing time. In order to make the study feasible the meta model optimization technique developed my Arie, M for manifold microgroove heat exchangers will be used. (Arie. M, 2012) For increased speed we are simulating one channel with one manifold for a single pass. A matlab script was created that generated the fluent and gambit journal files from the sampling points provided. A model validation as done comparing the sampling method with a full CFD model, the results are presented in Table 8

Table 8 Validation of Single Channel Model

Validation Data Point											
	Re	**Hch**	**aplh**	**Wch**	**Win**	**Hman**	**n**	**Wman**	**H_BaseV2**	**Pump_Tot**	**% diff**
Full Model	110.77	1000	2	55	869	1017	81	200	47189	527	18.37%
Single Channel Model	110.77	1000	2	55	869	1017	81	200	48620.34	430.19	-3.03%

A parametric study was done for each variable to see what values should be tested. The parametric study will yield the max values for our study while the minimum values will be determined by manufacturing capability. After the minimum and maximum values we determined from the parametric study a sampling program was used

to generate 300 sampling points that spanned the min and max of the geometric values. These initial points we run through our Matlab script, the fluent results were recorded and the heat transfer density and pumping power density were calculated. The initial points along with the associated fluent results were then put in to a Meta Model program that uses our 300 sampling points to generate 16,000 points based on the relationships from the initial sampling points. From these 16,000 points the optimum points are calculated using an exterior penalty method. Since these optimum points are most likely not one of the initial 300 sampling points the optimum geometry is re run through the Matlab script and the error between the meta model and the fluent model is calculated. The new fluent results for the optimum points are added to the Meta Model. This last step is repeated until the average error for the optimum points is reduced to acceptable values. Next we will look at the parametric study results.

5.3 Parametric Study

A parametric study was performed in order to determine the maximum values for the manifold and microgroove geometry. The range of values that were tested are listed in Table 9

Table 9 Range of Values Geometric Values for Parametric Study

Variable	Min	Max	Average
Re [-]	100	1000	550
Hch [μm]	200	1000	600
Alph [-]	0.2	2	1.1
Wch [μm]	20	60	40
Win [μm]	200	2000	1100
Hman [μm]	1000	2500	1750
N [-]	80	400	240
Wman [μm]	200	1200	700

One variable was changed at a time while the other variables were kept at the average values. From the parametric study results the maximum values for the sampling run were determined. The maximum and minimum values are listed in Table 10.

Table 10 Minimum and Maximum Values for Manifold and Microgroove Geometry

Variable	Min	Max
Re [-]	100	1000
Hch [μm]	500	2500
alph	0.2	2
Wch [μm]	40	100
Win [μm]	400	2000
Hman [μm]	500	2000
N [-]	80	500
Wman [μm]	500	
Hbase [μm]	400	

From the parametric study we were able to determine that the Wman had very little effect on pumping power and heat transferred. The relationship for heat transfer density and pumping power density in relation to Wman is shown in Figure 27. We can see what Wman has no effect on pumping power density and heat transfer density increases as Wman decreases. We have chosen Wman to be 500um because it allows for the most heat transfer density and is also easy to manufacture.

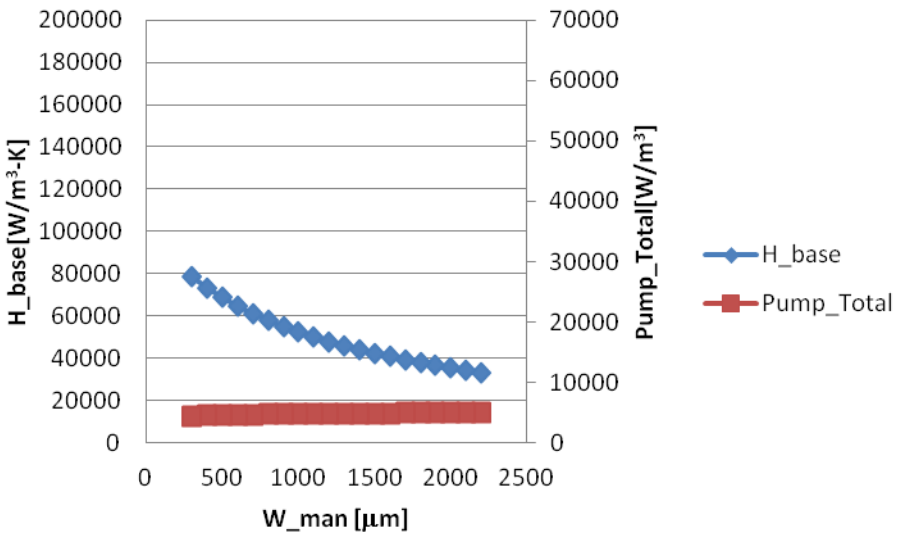

Figure 27 Heat Transfer Density and Pumping Power Density vs Wman

From the results that we calculated here we ran optimization sampling for 300 points. In the next section we will talk about the results that we got from the optimization program.

5.4 Optimization Results

The sampling points were input in to the metamodel and 16,000 points were created from that and plotted, pumping power density vs heat transfer density.

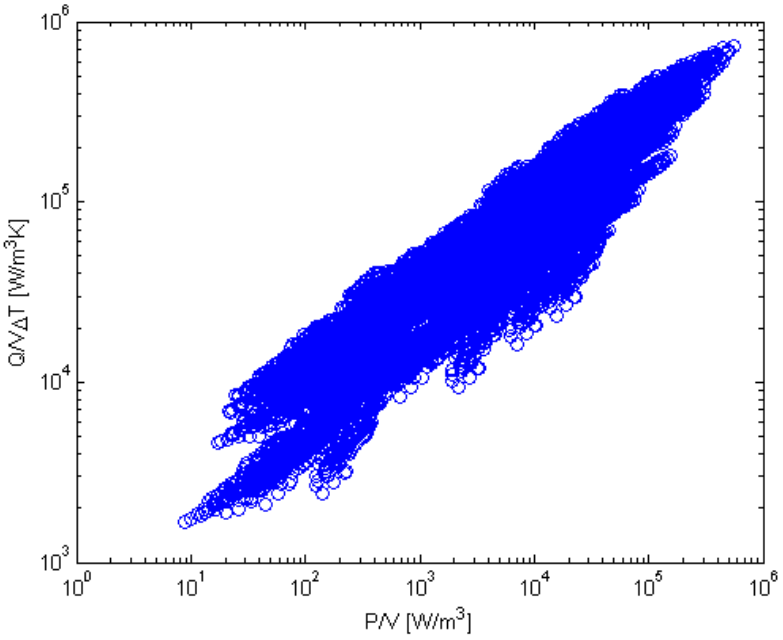

Figure 28 Optimization Study Feasible Domain

Figure 28 shows the feasible domain for the optimization study. This is the entire set of points that is feasible for the study. The optimum points will lay along the top of this curve because they allow for the most heat transfer for a given pumping power. Figure 29 shows the Pareto curve plotted on top of the feasible domain. 105 optimum points were generated using an exterior penalty method optimization technique.

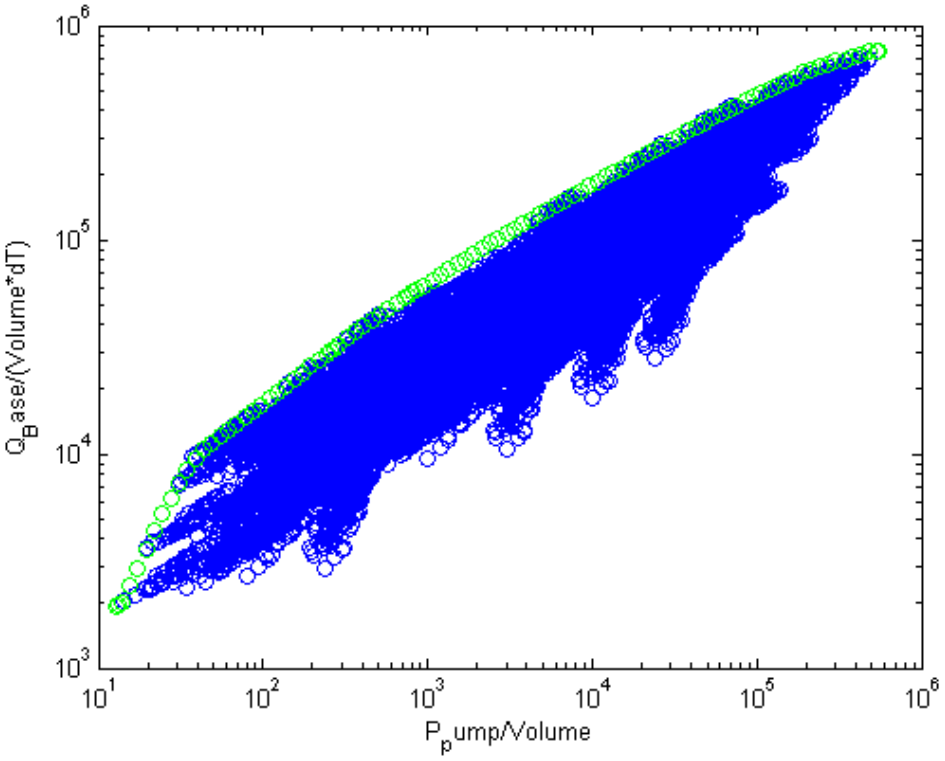

Figure 29 Optimization Study First Set of Optimum Points, Pareto Curve

These optimum points were generated using the metamodel and therefore are not actual CFD results. These optimum points were run through the sampling code and the pumping power density and heat transfer density were compared to see how close the metamodel results match the CFD results. The average error for heat transfer density and pumping power density on the first run were 13% and 30% respectively. After putting the optimum point results from the CFD code in to the metamodel a second set of optimum points were generated. The Pareto curve for the second set of optimum points is show in Figure 29. The average error for heat transfer density and pumping power density for the second set was 0.86% and 2.14% respectively. When the optimum points microchannel and manifold area ratio are compared to the manifolds from the experimental study the optimized manifolds microchannel area never exceeds 5 times the manifold area compared to 150 and 75 for Manifolds A and B respectively. This shows

that the manifolds can be designed more efficiently to increase heat transfer coefficient and reduce pressure drop and maldistribution.

Chapter 6: Conclusions and Suggested Future Work

A condenser is an essential part of any two-phase energy conversion system. Although microchannel condensers with millimeter scale hydraulic diameter of channels are currently penetrating many areas of energy conversion, further reduction in the channel size is being limited by the high pressure drop of such systems if not properly designed.

New way forward was shown by the University of Maryland's Smart and Small Thermal Systems (S2TS) laboratory introducing manifold microchannels for performance enhancement of condensers. That solved pressure drop issue however was used for small scale condenser for electronics cooling. The current work represents the first attempt to scale up manifold microchannel condenser to the scale of automotive and airspace applications.

An innovative design of tubular manifold microchannel condenser was developed, fabricated, and tested with two different manifold designs and two refrigerants over a parametric range of operation conditions of interest to the targeted application.

It was demonstrated that the current condenser design has a clear performances enhancement when compared to majority of commercial and researched condensers and represents drastically lower pumping power requirements, due to better utilization of the condensing heat transfer surface area, as well as minimizing any flow maldistribution of the condensing vapor.

In the current design flow area of manifold was almost two order of magnitudes higher when compared to the microchannel flow area therefore condensation flow

through microchannels was mostly dominated by manifold pressure drop. Decreasing microchannel area 3 times improves flow distribution and significantly improves condensation heat transfer.

Single-phase manifold microchannel heat transfer optimization corresponding to condenser air–side heat exchanger supported the requirement of optimum balance of manifold and microchannel flow areas, indicating that microchannel flow area should exceed manifold area more than 5-10 times.

Future Work

Designing and fabrication of condenser based on the findings of this research.

Developing of numerical tool for optimization of condensation process in manifolded microchannels.

References

Agarwal A, Garimella S. Representative Results for Condensation Measurements at Hydraulic Diameters ~100 Microns. J. Heat Transfer. 2010;132(4):041010-041010-12. doi:10.1115/1.4000879.

Arie, M. A., 2012, "Numerical Modeling and Optimization of Single Phase Manifold-Microchannel Plate Heat Exchanger," Master of Science, University of Maryland College park.

Cavallini, A. Censi, G. Del Col, D. Doretti, L. Longo, G.A. Rossetto. L, Experimental investigation on condensation heat transfer and pressure drop of new HFC refrigerants (R134a, R125, R32, R410A, R236ea) in a horizontal smooth tube, International Journal of Refrigeration, Volume 24, Issue 1, January 2001, Pages 73-87

Cetegen, E., 2010, "Force fed microchannel high heat flux cooling utilizing microgrooved surfaces," University of Maryland, College Park, Md.

Chang Yong Park, Pega Hrnjak, CO2 flow condensation heat transfer and pressure drop in multi-port microchannels at low temperatures, International Journal of Refrigeration, Volume 32, Issue 6, September 2009, Pages 1129-1139, ISSN 0140-7007

Ebrahim Al-Hajri, Amir H. Shooshtari, Serguei Dessiatoun, Michael M. Ohadi, Performance characterization of R134a and R245fa in a high aspect ratio microchannel condenser, International Journal of Refrigeration, Volume 36, Issue 2, March 2013, Pages 588-600, ISSN 0140-7007

Fernández-Seara, J., Uhía, F. J., Sieres, J., and Campo, A., 2007, "A general review of the Wilson plot method and its modifications to determine convection coefficients in heat exchange devices," Applied Thermal Engineering, 27(17–18), pp. 2745-2757.

Mahefkey, T., Yerkes, K., Donovan, B., and Ramalingam, M., "Thermal Management Challenges For Future Military Aircraft Power Systems," SAE Technical Paper 2004-01-3204, 2004, doi:10.4271/2004-01-3204.

Mandel. R, 2013, Personal Correspondence

Melanie Derby, Hee Joon Lee, Yoav Peles, Michael K. Jensen, Condensation heat transfer in square, triangular, and semi-circular mini-channels, International Journal of Heat and Mass Transfer, Volume 55, Issues 1–3, 15 January 2012, Pages 187-197, ISSN 0017-9310

Na Liu, Jun Ming Li, Jie Sun, Hua Sheng Wang, Heat transfer and pressure drop during condensation of R152a in circular and square microchannels, Experimental

Thermal and Fluid Science, Volume 47, May 2013, Pages 60-67, ISSN 0894-1777,

Recent Work on Boiling and Condensation in Microchannels Ping Cheng, Guodong Wang, and Xiaojun Quan, J. Heat Transfer 131, 043211 (2009), DOI:10.1115/1.3072906

SRINIVAS GARIMELLA (2004): Condensation Flow Mechanisms in Microchannels: Basis for Pressure Drop and Heat Transfer Models, Heat Transfer Engineering, 25:3, 104-116

Sung-Min Kim, Issam Mudawar, Theoretical model for annular flow condensation in rectangular micro-channels, International Journal of Heat and Mass Transfer, Volume 55, Issue 4, 31 January 2012, Pages 958-970, ISSN 0017-9310

Sung-Min Kim, Joseph Kim, Issam Mudawar, Flow condensation in parallel micro-channels – Part 1: Experimental results and assessment of pressure drop correlations, International Journal of Heat and Mass Transfer, Volume 55, Issue 4, 31 January 2012, Pages 971-983

Swain, E.F., "Aircraft Avionics Cooling, Present And Future," Proceedings of the IEEE 1998 National Aerospace and Electronics Conference, 1998. NAECON 1998.

U.S. Energy Information Administration, "Annual Energy Outlook 2013 Early Release" http://www.eia.gov/forecasts/aeo/er/pdf/0383er(2013).pdf

Wang, W., and Wang, X., "Experiments of Condensation Heat Transfer in Micro Channel Heat Exchanger" (2010). International Refrigeration and Air Conditioning Conference. Paper 1082.